

Symplectic Maps for Diverted Plasmas

I. L. Caldas¹, B. F. Bartoloni², D. Ciro³, G. Roberson⁴, A. B. Schelin⁵, Tiago Kroetz⁶, Marisa Roberto⁴, Ricardo L. Viana³, Kelly C. Iarosz¹, Antonio M. Batista⁷, Philip J. Morrison⁸

¹Instituto de Física, Universidade de São Paulo, São Paulo, SP, Brazil.

²Departamento de Ensino Geral at Faculdade de Tecnologia de São Paulo, São Paulo, Brazil.

³Departamento de Física, Universidade Federal do Paraná, Curitiba, PR, Brazil.

⁴Aeronautics Institute of Technology at CTA, São José dos Campos, Brazil.

⁵Institute of Physics at University of Brasília, Brasília, Brazil.

⁶Department of Mathematics at Federal Technological University of Paraná, Pato Branco, Brazil.

⁷Departamento de Matemática e Estatística, Universidade Estadual de Ponta Grossa, Ponta Grossa, PR, Brazil.

⁸Institute for Fusion Studies at The University of Texas at Austin, USA.

Corresponding author: ibere@if.usp.br

Abstract

Nowadays, divertors are used in the main tokamaks to control the magnetic field and to improve the plasma confinement. In this article, we present analytical symplectic maps describing Poincaré maps of the magnetic field lines in confined plasmas with a single null poloidal divertor. Initially, we present a divertor map and the tokamap for a diverted configuration. We also introduce the Ullmann map for a diverted plasma, whose control parameters are determined from tokamak experiments. Finally, an explicit, area-preserving and integrable magnetic field line map for a single-null divertor tokamak is obtained using a trajectory integration method to represent toroidal equilibrium magnetic surfaces. In this method, we also give examples of onset of chaotic field lines at the plasma edge due to resonant perturbations.

keywords: magnetic surfaces, symplectic map, divertor

1 Introduction

Tokamaks are the most promising devices to confine fusion plasmas [1, 2]. The plasma confinement depends on the magnetic field which determines the particle transport [3]. To the leading order approximation, the charged particles follow the magnetic field lines [2, 3]. Thus, the particle transport can be controlled by properly modifying the magnetic field as a result of electrical currents in external coils and also by installing poloidal divertors [1, 4]. Such divertors are used to control the plasma impurity content [5, 6] and have a special magnetic configuration created by electric currents in external coils, such that the field lines have escape channels, through which plasma particles can be diverted out of the tokamak wall and redirected to divertor plates.

Divertors are essential components in modern tokamaks, such as ITER [1, 7]. The overlap of the magnetic fields created by the divertor with the magnetic field of the plasma creates a hyperbolic fixed point where the poloidal magnetic field is null. The hyperbolic point is in the separatrix, the invariant line separating the plasma, with stable and unstable manifolds [8, 9]. Outside the separatrix the magnetic field lines intersect the collector plates [1].

The tokamak map trajectories can be obtained by directly integrating the field line differential equations, but the integration requires a time-consuming calculation which may not be appropriate for studying long-term of the field behavior. Therefore, approximated maps have to be considered if one wants to have the advantage of much shorter computation times [3, 10, 11]. Analytical tokamak maps can be derived from physical models and mathematical approximations applied to the field line equations, or even can be ad hoc maps to obtain a qualitative or quantitative description of the physical situation that they describe [11, 12, 13].

Magnetic field lines are, in general, orbits of Hamiltonian systems of one-and-a-half degrees of freedom with a time-like periodic coordinate. Consequently, the field line configuration can be represented in Poincaré sections at a fixed toroidal angle, equivalent to two-dimensional area-preserving maps [3, 10, 11]. Thus, we can use such maps to qualitatively represent the magnetic configurations of tokamak plasmas [14]. In this work, we present maps proposed to investigate the fundamental features of the magnetic field line dynamics in tokamaks with divertor. We introduce new versions of the Tokamak and Ullmann map for tokamaks with divertor and review the Divertor Map and an integrable map for equilibrium divertor configuration in toroidal geometry.

The paper is organized as follows: in Section 2, we show the tokamak divertors. In Section 3, we introduce three symplectic maps: the Divertor Map, the Tokamak map for divertor configuration, and the Ullmann map for divertor. We also give examples of these maps to show their dynamical characteristics. In Section 4, we introduce an integrable map to simulate toroidal magnetic surfaces modified by a divertor. Section 5 contains the conclusions.

2 Divertor

In tokamaks, a material limiter separates the plasma column from the wall. However, to improve the plasma isolation and eliminate impurities, divertors have been used in several modern tokamaks and will be used in ITER [7]. Divertors consist of conductors arranged externally, that carry specific electric currents to create X point (or hyperbolic fixed point) where the poloidal magnetic field is null, due to the overlap of the magnetic fields of the conductors with the magnetic field of the plasma.

In Fig. (1), we present an example of the magnetic surfaces in a tokamak with divertor. In this figure, the separatrix in red, with one hyperbolic point, separates the internal toroidal magnetic surfaces with quasi-periodic lines of the external surfaces with open field lines. Moreover, from the X point arises a

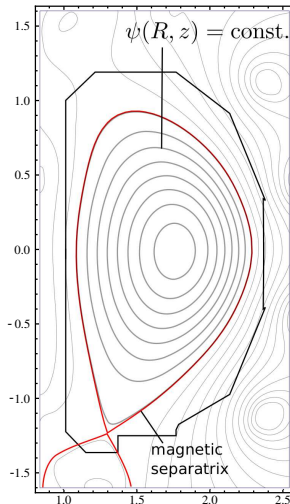


Figure 1: (Color online) Schematic view of a tokamak divertor equilibrium configuration with intersection of invariant magnetic surfaces on a plane determined by a specific toroidal angle. The red line indicates the magnetic separatrix while the contours are magnetic surfaces.

separatrix with two manifolds, one stable and the other unstable.

Several tokamaks with divertors have non-axisymmetric resonant perturbation coils designed specifically to modify the plasma magnetic field [1, 2]. One of the actions of the resonant perturbations created by these coils is to create chaotic magnetic field layers in the peripheral region of the plasma column [7, 11, 13].

In Fig. (2), we show an example of this kind of coils arranged around a tokamak chamber, similar to the coils used in DIII-D tokamak [15]. To show how the tokamak equilibrium is perturbed by the coils of Fig. (2), we present in Fig. (3), the transversal cross section of the diverted tokamak magnetic field lines for a set of control parameters commonly found in tokamak discharges [15, 16]. In Fig. (3) we can see chaotic lines and magnetic islands around the divertor hyperbolic point, the separatrix of the unperturbed diverted field, and the divertor plates where the chaotic lines intersect the tokamak chamber.

The chaotic layer at the plasma edge affects the plasma confinement [17] and can be controlled by the perturbation introduced by the divertor [7]. The chaotic layer in this region is mainly determined by the manifolds from the hyperbolic point [18].

3 Symplectic Maps

Symplectic maps have been commonly used in physics to describe Poincaré sections of dynamical systems [19, 20, 21]. In plasma physics, a pioneer sym-

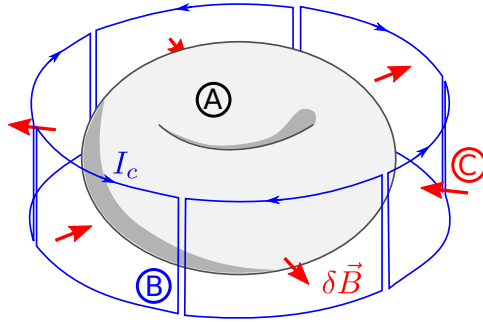


Figure 2: (Color online) Schematic view of a tokamak vacuum chamber (A), and the external coils (B), responsible for the resonant magnetic field (C). Blue lines indicate the perturbing external currents and the red vectors the non-axisymmetric field perturbation.

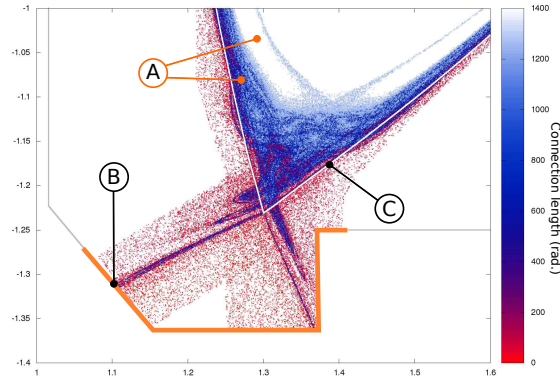


Figure 3: (Color online) Detail of the Poincaré map of the perturbed field lines in the magnetic saddle region. The magnetic perturbation leads to the formation of a peripheral chaotic layer and magnetic islands (A). Chaotic field lines now cross the symmetric separatrix (C), and the open field lines intersect the tokamak chamber (B) in asymmetric patterns controlled by the invariant manifolds of the saddle.

plectic map to describe particle orbits for stellarators was introduced in [22]. After that, symplectic maps have been used to investigate particle transport in magnetically confined plasmas [23, 24, 25]. Symplectic maps have also been introduced to investigate the chaotic field lines in tokamaks. The first one was the Martin-Taylor map introduced to describe the perturbation created by the ergodic magnetic limiter in tokamaks [26].

In this section, we present symplectic maps to describe the diverted magnetic field lines in tokamaks: the Divertor Map introduced in [27] and new versions of the Tokamak [28] and the Ullmann's map [29] for divertors. These maps are

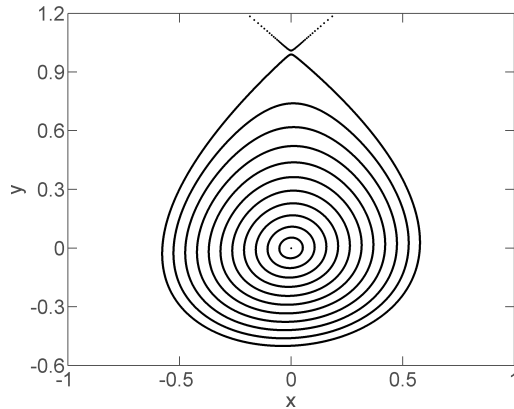


Figure 4: Poincaré map of the Divertor Map for $k = 0.6$, depicting the stable fixed point at $(0,0)$ and some invariant curves. Closed invariant lines are separated from open lines (not shown) by the separatrix, which includes the hyperbolic point at $(0,1)$.

nonintegrable and describe plasma equilibrium with chaotic layers, around the hyperbolic point, due to resonant perturbations.

3.1 Divertor Map

The first Divertor Map has been presented as the simplest model for the magnetic configuration of a tokamak equipped with a divertor. The map simulates Poincaré sections of field lines [27].

The Divertor Map introduced in [27] is

$$\begin{aligned} x_{n+1} &= x_n - ky_n(1 - y_n), \\ y_{n+1} &= y_n + kx_{n+1}, \end{aligned} \tag{1}$$

where (x_n, y_n) are the rectangular coordinates on the poloidal surface of section and the control parameter k determines both the safety factor and the strength of toroidal asymmetries in the magnetic field. In this map, the equilibrium and perturbation are not separable.

For small values of the control parameter k , the map shows the formation of a thin chaotic layer in the separatrix region, whose chaotic orbits eventually reach the plates, which are set in the numerical simulations at $y_{\text{plate}} = 1$. One example is in Fig. (4) for $k = 0.6$.

3.2 Tokamap for Diverted Plasmas

The Tokamap has been introduced to describe field lines of a tokamak equilibrium modified by a resonant perturbation. There are several versions of this

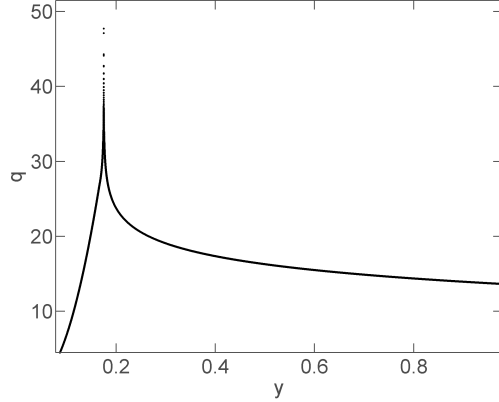


Figure 5: Safety factor profile considered for the Tokamap to obtain Fig. (6). The coordinate y corresponds to the radial coordinate used in large aspect ratio tokamaks.

map to account for different equilibria and perturbations. Here, we consider the following version of the map for tokamak plasmas [28]:

$$\begin{aligned}\psi_k &= \psi_k - \frac{L}{2\pi} \frac{\psi_{k+1}}{1 + \psi_{k+1}} \sin(2\pi\theta_k), \\ \theta_{k+1} &= \theta_k + \frac{1}{q(\psi_{k+1})} - \frac{L}{2\pi} \frac{1}{(1 + \psi_{k+1})^2} \cos(2\pi\theta_k),\end{aligned}\quad (2)$$

where L is a control parameter that simulates the resonant perturbation amplitude and q is the safety factor that characterizes the tokamak equilibrium.

Here, we consider a safety factor profile q , as considered in [30], with a singularity at $r = r^*$. This profile is polynomial for $0 \leq r < r_{95}$ and logarithmic for $r_{95} < r \leq r^*$, where $r_{95} = 0.95r^*$:

$$q_0(r) = q_a + c_1 r + c_2 + r^2, \quad \text{if } r \leq r_{95}, \quad (3)$$

$$q_0(y) = \alpha \ln(y^* - y) + \beta, \quad \text{if } r_{95} \leq r. \quad (4)$$

We choose the q profile parameters such that: $q_0=11.1$, $q_{95}=3.3$, $r^*=0.18$, $r_{95}=0.171$, and $r_{95}, s_{95}=110.8$ is related to magnetic shear for the reference surface r_{95} . The considered profile is shown in Fig. (5). In Fig. (6), we show invariant and chaotic lines, around the hyperbolic point, for the control parameter $L=e^{-1}$. The observed chaotic layer appears in the resonant region.

3.3 Ullmann Map for Diverted Plasma

A special set of coils, known as the ergodic limiter, have been proposed to create a chaotic layer at the tokamak plasma edge in order to separate the plasma from

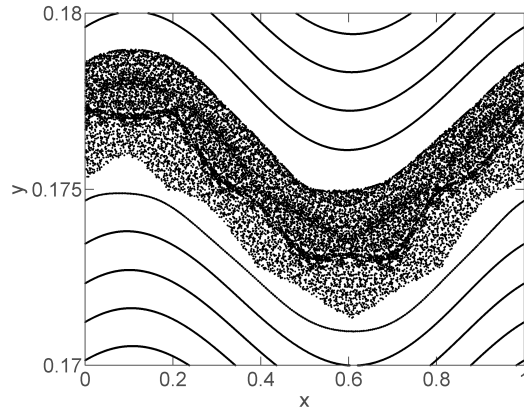


Figure 6: Invariant magnetic surfaces and chaotic field lines obtained from the Tokamap for $L = 0.1$.

the wall [4]. Since then different kinds of limiters were installed in tokamaks to control the plasma confinement [12, 13, 31].

In [29] a symplectic map was proposed to describe tokamak field lines perturbed by an ergodic limiter. The map is valid for large aspect ratio tokamaks with toroidal correction. In this approximation, the toroidal coordinate is related to z . In the model, the topology of the magnetic field lines is described by a Poincaré map in the section $z = \text{constant}$, with variables r_n, Θ_n denoting the coordinates of the n th intersection of the field line on the considered section [12, 29].

The analytical expressions for the Poincaré map is obtained, for the equilibrium with toroidal correction, by the generating function:

$$G_{\text{TO}}(r_n, \theta_n) = G_{\text{cil}}(r_n, \theta_n) + \sum_{l=1}^{\infty} a_l \left(\frac{r_n}{R_0} \right)^l \cos^l \theta_n \quad (5)$$

and the following relations:

$$r_n = \frac{\partial G_{\text{TO}}(r_n, \theta_n)}{\partial \theta_n}, \quad (6)$$

$$\theta_n = \frac{\partial G_{\text{TO}}(r_n, \theta_n)}{\partial r_n}. \quad (7)$$

From equations (6) and (7) we obtain the map expressions

$$r_{n+1} = \frac{r_n}{1 - a_1 \sin \theta_n}, \quad (8)$$

$$\theta_{n+1} = \theta_n + \frac{2\pi}{q(r_{n+1})} + a_1 \cos \theta_n, \quad (9)$$

where a_1 is a correction due to the toroidal effect and $q(r)$ is the safety factor profile. The toroidal correction introduces a poloidal angle θ dependence on the map. Such correction, considered in the model, takes into account the outward magnetic surface displacement, characteristic of tokamak equilibria in toroidal geometry. The constant $a_1 = -0.04$ was fit to reproduce the observed tokamak magnetic surface displacements [29]. Since the map is derived from a generating function, interpreted as a canonical transformation between the previous and the next coordinates, the Jacobian for this map is unitary and, consequently, the map is symplectic [12, 29].

We consider the same safety factor profile q_0 considered for the Tokamak, with a singularity in the same position and the same parameters $q_0 = 11.1$, $q_{95} = 3.3$, $r^* = 0.18$, $r_{95} = 0.171$ and the magnetic shear, for the reference surface $r_{95}, s_{95} = 110.8$.

Neglecting the toroidal correction, i.e., for $a_1 = 0$, the map is integrable and the rotation number profile is the inverse of the safety factor q_0 appearing in equations (3) and (4) with a divergence at $r = r^*$. However, including the predicted toroidal correction and considering $a_1 = -0.04$, mentioned before, the rotation number has to be calculated numerically by the expression

$$q = \frac{1}{l} \rightarrow q \equiv \lim_{k \rightarrow \infty} \frac{2\pi k}{\sum_{j=0}^k (\theta_{j+1} - \theta_j)}. \quad (10)$$

In Fig. (7), we have the analytical safety factor profile obtained from this definition and, for initial conditions with a fixed θ , the modified safety factor calculated numerically for 100 values of r between 0 and 1. We see in Fig. (7) the difference between the original profile inserted in equation (9) and the one calculated, considering the toroidal correction, by applying equation (10). As shown in [12] and [29], we can add another symplectic map as an external perturbation to obtain a chaotic layer on the resonant region.

4 Integrable Map for toroidal Magnetic Surfaces

In this section, we introduce a procedure to obtain an integrable map simulating a plasma equilibrium for a diverted tokamak [30, 32, 33].

To obtain the desired map it is necessary, initially, to find a potential $V(x)$ that produces a topology with an X-point, with a Hamiltonian ψ given by

$$\psi = \frac{y^2}{2} + V(x). \quad (11)$$

In the plasma map this Hamiltonian will be the flux function. We choose a double-well shaped potential to create curves in phase space that exhibit two closed regions delimited by a separatrix between them with an X point. The expression for $V(x, y)$ with the desired properties will be written as a set of six parabolas, indicated in Fig. (8a), joined smoothly the connection points. Figure (8a) shows the chosen potential profile used in this article [32]. The position

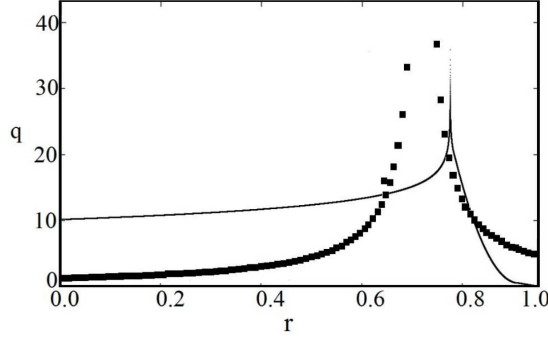


Figure 7: Analytical safety factor profile, obtained from equations (3) and (4), with a divergence at $r = r^*$, and the safety factor profile calculated numerically, for $\theta = y = 0.05$. The coordinate r is normalized to a (plasma radius).

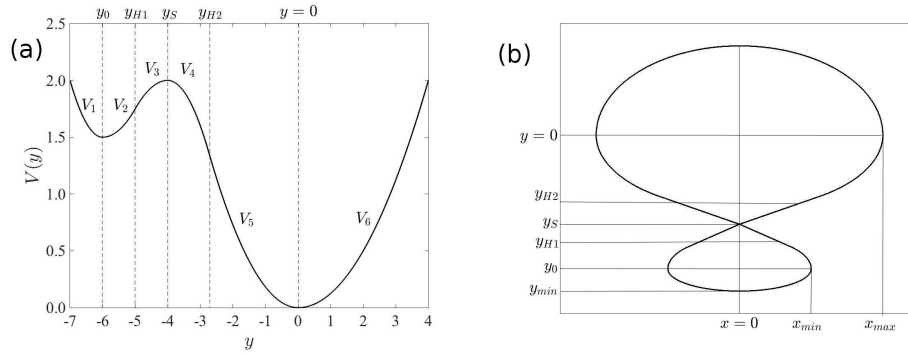


Figure 8: (a) Potential used to obtain the magnetic surfaces. (b) Schematic view of a separatrix in rectangular coordinates indicating the meaning of each geometric parameter related to $V(y)$ for the normalized geometric parameters $x_{\max} = -2$, $x_{\min} = -1$, $y_{\min} = 7$, $y_{\max} = 4$, $y_{H1} = 5$, $y_{H2} = 2.75$, $y_S = 4$, $y_0 = 6$.

$y = 0$ corresponds to the plasma center. In Fig. (8b), we present the separatrix for the orbits obtained for the chosen potential of Fig. (8a). This separatrix determines, in the map, the last closed magnetic surfaces inside the plasma.

We choose an analytical expression for the potential represented in Fig. (8a). For this potential, the trajectory corresponding to the separatrix is shown in Fig. (8b), for ITER parameters.

The next step is to solve Hamilton's equations to get x and y in terms of

their initial conditions (x_0, y_0) and time t ,

$$\frac{dx}{dt} = -\frac{\partial\psi}{\partial y}, \quad (12)$$

$$\frac{dy}{dt} = \frac{\partial\psi}{\partial x}. \quad (13)$$

The continuous equations are transformed into a discrete map, where the continuous time parameter t is turned into a discrete time step Δ :

$$x(x_0, y_0, t) = x_{n+1}(x_n, y_n, \Delta), \quad (14)$$

$$y(x_0, y_0, t) = y_{n+1}(x_n, y_n, \Delta). \quad (15)$$

To obtain the magnetic surfaces we choose Δ given by the inverse of the safety factor

$$\Delta = \frac{T(\psi)}{q(\psi)}. \quad (16)$$

where $T(\psi)$ is the rotation period of the invariant curves associated with the continuous system and $q(\psi)$ is the safety factor of the magnetic surface we intend to represent by the invariant curve [32, 33].

We choose a monotonic safety factor profile similar to the one used before in Section 3 (B) and (C) expressed in terms of the function ψ [32]:

$$q(\psi) = \begin{cases} q_0 + c_1\psi + c_2\psi^2, & \psi \leq \psi_{95}, \\ \alpha \ln(\psi_S - \psi) + \beta, & \psi > \psi_{95}. \end{cases}$$

In the numerical examples we choose the safety factor parameters such that the magnetic shear at the reference surface, defined as

$$\hat{s}_{95} = \left. \frac{r_{95}}{q_{95}} \frac{dq}{dr} \right|_{r_{95}}, \quad (17)$$

are $\hat{s}_{95} = 110.8$ and $q_{95} = 3.3$.

For each line, the value of ψ is given by $\psi = \psi(x_0, y_0)$. At each point (x_0, y_0) , ψ determines the Δ value:

$$\Delta = \Delta(\psi). \quad (18)$$

The map gives the Poincaré map on the surface $\varphi = 0$

$$M_\Delta(x_n, y_n) = (x_{n+1}, y_{n+1}). \quad (19)$$

The magnetic surfaces are shown in Fig. (9).

To perturb the divertor integrable map, we apply the symplectic Martin-Taylor map [26], that simulates the effect of an ergodic limiter in large aspect-ratio tokamaks, which introduces external symmetry-breaking resonances, so as to generate a chaotic region near the separatrix passing through the X-point.

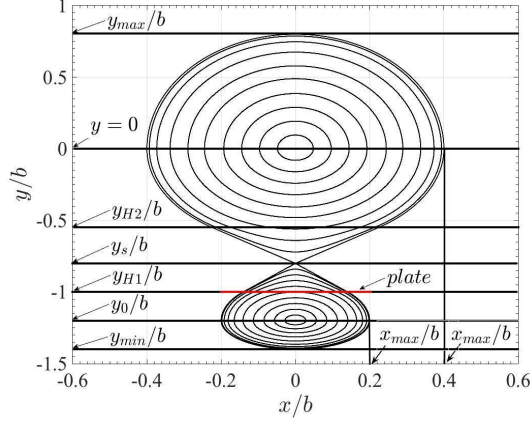


Figure 9: (Color online) Invariant magnetic surfaces obtained from the integrable map for the chosen parameters indicated in the text.

For each toroidal turn, the Martin Taylor map is applied at the $\varphi = 0$ surface as a kick perturbation:

$$(x^*, y^*) = M_{\Delta_n}(x_n, y_n), \quad (20)$$

$$(x_{n+1}, y_{n+1}) = P(x^*, y^*). \quad (21)$$

Thus, the map used to describe the perturbation of an external resonant helical perturbation due to a magnetic limiter is given by [26]

$$x_{n+1} = x_n - ce^{-\frac{my_n}{r_c}} \cos\left(\frac{mx_n}{r_c}\right), \quad (22)$$

$$y_{n+1} = y_n + \frac{r_c}{m} \log \left\{ \cos \left[\frac{mx_n}{r_c} - ce^{-\frac{my_n}{r_c}} \cos \left(\frac{mx_n}{r_c} \right) \right] \right\} \\ - \frac{r_c}{m} \log \left\{ \cos \left(\frac{mx_n}{r_c} \right) \right\}, \quad (23)$$

where the parameter c quantifies the perturbation strength, proportional to the current in the limiter coils, s is the magnetic shear at the plasma edge, and r_c is the plasma radius. The composed field line map is used to obtain the perturbed field line configurations, shown in Fig. (10), with different magnetic shear profiles at the plasma edge for the control parameters $s = 1.9$ and $s = 2.5$ for $c = 3$. The current in the ergodic limiter is the same in Figs. (10a) and (10b).

The introduced non-axisymmetric stationary magnetic perturbation leads to the formation of homoclinic tangles near the divertor magnetic saddle [18]. These tangles intersect the divertor plates in static helical structures.

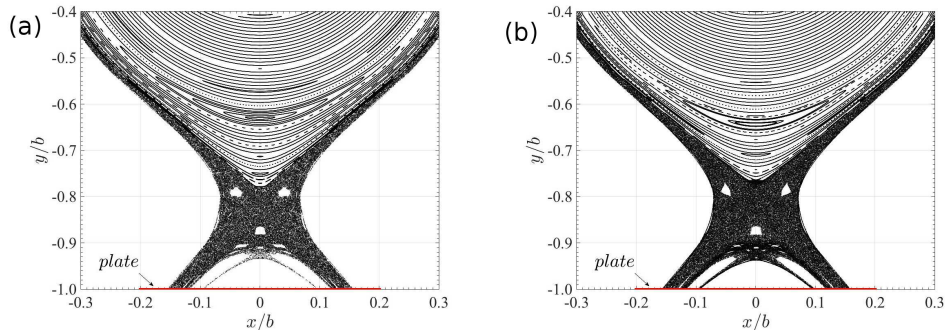


Figure 10: (Color online) Phase portrait for the total field line map. (a) $s = 1.9$ and $p = 3$, (b) $s = 2.5$ and $p = 3$.

5 Conclusions

To describe Poincaré sections of diverted magnetic field lines, we presented two-dimensional symplectic maps, in the limit of large aspect ratio simulating the alterations the magnetic topology caused by the divertor.

These maps can be used to investigate the main characteristics of the chaotic layer around the hyperbolic point introduced by divertors, and how these characteristics change with the equilibrium and perturbation control parameters. The Tokamap and Ullmann map were presented in new versions for tokamaks with divertor. We also presented a map describing magnetic surfaces in toroidal geometry.

All the maps introduced in this article are useful for studying different aspects of the field line dynamics and transport in tokamaks with divertor. Extensions of the presented maps could be derived to include additional effects not considered in this article, such as the particle's finite Larmor radius [34, 35] and the screening caused by the plasma response to resonant magnetic perturbations [36, 37].

Acknowledgments

This work was partially supported by the National Council for Scientific and Technological Development (CNPq)-Brazil, grants 870198/1997-1 and 830577/1999-8 and the São Paulo Research Foundation (FAPESP) grants 2012/18073-1, 2015/07311-7 and 2011/19296-1. PJM was supported by the U.S. Department of Energy Contract No.DE-FG05-80ET-53088.

References

- [1] C. W. Horton, Jr. S. Benkadda, *ITER Physics*, 1nd ed., Singapore, MY: World Scientific Publishing, 2015, pp. 248.
- [2] C. W. Horton, *Turbulent Transport in Magnetized Plasmas*, 1nd ed., New Jersey, USA: World Scientific Publishing, 2012, pp. 520.
- [3] R. D. Hazeltine, J. D. Meiss, *Plasma Confinement*, 1nd ed., New York, USA: Dover Books on Physics, 2003, pp. 480.
- [4] F. Karger, K. Lackner, “Resonant helical divertor,” *Phys. Lett. A*, vol. 61, pp. 385-387, Jun. 1977.
- [5] F. Wagner, G. Becker, K. Behringer, D. Campbell, A. Eberhagen, W. Engelhardt, G. Fussmann, O. Gehre, J. Gernhardt, G. V. Gierke, G. Haas, M. Huang, F. Karger, M. Keilhacker, O. Klüber, M. Kornherr, K. Lackner, G. Lisitano, G. G. Lister, H. M. Mayer, D. Meisel, E. R. Müller, H. Murmann, H. Niedermeyer, W. Poschenrieder, H. Rapp, H. Röhr, F. Schneider, G. Siller, E. Speth, A. Stäbler, K. H. Steuer, G. Venus, O. Vollmer, and Z. Yü, “Regime of Improved Confinement and High Beta in Neutral-Beam-Heated Divertor Discharges of the ASDEX Tokamak,” *Phys. Rev. Lett.*, vol. 49, no. 19, pp. 1408-1414, Nov. 1982.
- [6] M. Kikuchi, K. Lackner, M. Q. Tran, *Fusion Physics*, 1nd ed., Vienna, AT: IAEA, 2012, pp. 1129.
- [7] ITER Physics Expert Group on Divertor, “Power and Particle Control,” *Nucl. Fusion*, 1999, ch. 4, vol. 39, pp. 2391-2469.
- [8] T. E. Evans, R. A. Moyer, and P. Monat, “Modeling of stochastic magnetic flux loss from the edge of a poloidally diverted tokamak,” *Phys. Plasmas*, vol. 9, pp. 4957-4967, Nov. 2002.
- [9] E. C. da Silva, I. L. Caldas, R. L. Viana, and M. A. F. Sanjuán, “Escape patterns, magnetic footprints, and homoclinic tangles due to ergodic magnetic limiters,” *Phys. Plasmas*, vol. 9, pp. 4917-4928, Nov. 2002.
- [10] P. J. Morrison, “Magnetic Field Lines, Hamiltonian Dynamics, and Non-twist Systems,” *Phys. Plasmas.*, vol. 7, pp. 2279-2289, May. 2000.
- [11] S. S. Abdullaev, *Construction of Mappings for Hamiltonian Systems and Their Applications*, 2nd ed., Berlin: Springer-Verlag Berlin Heidelberg, vol. 691, 2006, pp. 379.
- [12] J. S. E. Portela, I. L. Caldas, R. L. Viana, “Tokamak magnetic field lines described by simple maps,” *Eur. Phys. J. Spec. Top.*, vol. 165, pp. 195-210, Dec. 2008.

- [13] I. L. Caldas, R. L. Viana, M. S. T. Araujo, A. Vannucci, E. C. da Silva, K. Ullmann, M. V. A. P. Heller, “Control of Chaotic Magnetic Fields in Tokamaks,” *Braz. J. Phys.*, vol. 32, no. 4, pp. 980-1004, Dec. 2002.
- [14] S. R. Barocio, E. Chávez-Alarcón, C. Gutierrez-Tapia, “Mapping the intrinsic stochasticity of tokamak divertor configuration,” *Braz. J. Phys.*, vol. 36, no. 2B, pp. 550-556, Jun. 2006.
- [15] D. Ciro, T. E. Evans, I. L. Caldas, “Modeling non-stationary, non-axisymmetric heat patterns in DIII-D tokamak,” *Nucl. Fusion*, vol. 57, no.016017, 2017.
- [16] C. G. L. Martins, M. Roberto, I. L. Caldas. “Delineating the magnetic field line escape pattern and stickiness in a poloidally diverted tokamak,” *Physics of Plasmas*, vol. 21, no. 082506, Jul. 2014.
- [17] A. Vannucci, I. L. Caldas, I. C. Nascimento, “Disruptive instabilities in the discharges of the TBR-1 small Tokamak,” *Plas. Phys. Control. Fusion*, vol. 31, pp. 147, Feb. 1989.
- [18] A. Wingen, T. E. Evans, and K. H. Spatschek, “High resolution numerical studies of separatrix splitting due to non-axisymmetric perturbation in DIII-D,” *Nucl. Fusion*, vol. 49, no. 5, pp. 055027, Apr. 2009.
- [19] J. D. Meiss, “Symplectic maps, variational principles, and transport,” *Rev. Mod. Phys.*, vol. 64, no. 3, pp. 795-848, Jul. 1992.
- [20] J. M. Greene, “A method for determining a stochastic transition,” *J. Math. Phys.*, vol. 20, no. 6, pp. 1183-1201, Jun. 1979.
- [21] B. V. Chirikov, “A universal instability of many-dimensional oscillator systems,” *Phys. Rep.*, vol. 52, no. 5, pp. 263-379, May. 1979.
- [22] M D. Kruskal, “Some properties of rotational transforms,” *AEC Report*, Springfield: VA, 1952, no. NYO-998, PM-S-5.
- [23] W. Horton, H-B. Park, J-M. Kwon, D. Strozzi, P. J. Morrison, D-I, Choi, “Drift wave test particle transport in reversed shear profile,” *Phys. Plasmas*, vol. 5, no. 11, pp. 3910-3917, Nov. 1998.
- [24] D. del Castillo-Negrete, P.J. Morrison, “Chaotic transport by Rossby waves in shear flow,” *Phys. Fluids A*, vol. 5, no. 4, pp. 948-965, Apr. 1993.
- [25] D. del Castillo-Negrete, J. Greene, P.J. Morrison, “Area preserving non-twist maps: periodic orbits and transition to chaos,” *Physica D*, vol. 91, pp. 1-23, Mar. 1996.
- [26] T. J. Martin and J. B. Taylor. “Ergodic behaviour in a magnetic limiter,” *Plas. Phys. Control. Fusion*, vol. 26, pp. 321-340, Mar. 1984.

- [27] A. Punjabi, A. Verma, A. Boozer, “Stochastic broadening of the separatrix of a tokamak divertor,” *Phys. Rev. Lett.*, vol. 69, no. 23, pp. 3322-3325, Dec. 1992.
- [28] R. Balescu, M. Vlad, F. Spineanu, “Tokamak: A Hamiltonian twist map for magnetic field lines in a toroidal geometry,” *Phys. Rev. E.*, vol. 58, pp. 951-964, Jul. 1998.
- [29] K. Ullmann, I.L. Caldas, “A symplectic mapping for the ergodic magnetic limiter and its dynamical analysis,” *Chaos, Solitons and Fractals*, vol. 11, no. 13, pp. 2129-2140, Oct. 2000.
- [30] T. Kroetz, M. Roberto, I. L. Caldas, R. L. Viana, P. J. Morrison, P. Abbamonte, “Integrable maps with non-trivial topology: application to divertor configurations,” *Nucl. Fusion*, vol. 51, no. 034003, Feb. 2010.
- [31] Ph. Ghendrih, A. Grosman, and H. Capes, “Theoretical and experimental investigations of stochastic boundaries in tokamaks,” *Plas. Phys. Control. Fusion*, vol. 38, no. 10, pp. 1653-1724, 1996.
- [32] T. Kroetz, M. Roberto, I. L. Caldas, R. L. Viana, P. J. Morrison, “Divertor map with freedom of geometry and safety factor profile,” *Plas. Phys. Control. Fusion*, vol. 54, no. 4, pp. 045007, Mar. 2012.
- [33] G. Roberson, M. Roberto, I. L. Caldas, T. Kroetz, R. L. Viana. “Shaping Diverted Plasmas With Symplectic Maps,” *IEEE Transactions on Plasma Physics*, vol. 45, no. 3, pp. 356-363, Feb. 2017.
- [34] J. J. Martinell and D. del-Castillo-Negrete, “Gyroaverage effects on chaotic transport by drift waves in zonal flows,” *Phys. Plasmas*, vol. 20, no. 022303, Feb. 2013.
- [35] J. D. da Fonseca, D. del-Castillo-Negrete, and I. L. Caldas. “Area-preserving maps models of gyroaveraged ExB chaotic transport,” *Phys. Plasmas*, vol. 21, no. 092310, Sep. 2014.
- [36] A. Wingen, N. M. Ferraro, M. W. Shafer, E. A. Unterbeg, J. M. Canik, T. E. Evans, D. L. Hillis, S. P. Hirshman, S. K. Seal, P. B. Snyder, and A. C. Sontag, “Connection between plasma response and resonant magnetic perturbation (RMP) edge localized mode (ELM) suppression in DIII-D,” *Plasma Phys. Control. Fusion*, vol. 57, no. 10, p. 104006, Sep. 2015.
- [37] A. C. Fraile Jr, M. Roberto, I. L. Caldas and Caroline G. L. Martins, “Plasma Response to Resonant Magnetic Perturbations in Large Aspect Ratio Tokamaks,” *IEEE Trans. Plas. Scien.*, vol. PP, pp. 1-7, no. 99, Oct. 2017.